

Laser-induced tissue hyperthermia mediated by gold nanoparticles: toward cancer phototherapy

Georgy S. Terentyuk

Saratov State University
Department of Optics and Biophotonics
83 Astrakhanskaya
Saratov 410012
Russia

Galina N. Maslyakova

Leyla V. Suleymanova
Saratov Medical State University
112 B. Kazachya
Saratov 410012
Russia

Nikolai G. Khlebtsov

Boris N. Khlebtsov
Russian Academy of Science
Institute of Biochemistry and Physiology of Plants
and Microorganisms
13 Prospekt Entuziastov
Saratov 410049
Russia

Garif G. Akchurin

Irina L. Maksimova
Saratov State University
Department of Optics and Biophotonics
83 Astrakhanskaya
Saratov 410012
Russia

Valery V. Tuchin

Saratov State University
Department of Optics and Biophotonics
83 Astrakhanskaya
Saratov 410012 Russia
and
Russian Academy of Science
Institute of Precise Mechanics and Control
24 Rabochaya
Saratov 410028
Russia

1 Introduction

The available hyperthermic techniques for cancer tumor therapy¹⁻⁴ possess low spatial selectivity in the heating of tumors and surrounding healthy tissues. One of the ways to improve the laser heating spatial selectivity is tumor tissue photothermal labeling by gold nanoparticles with different shapes and structures, such as nanoshells,⁵⁻⁷ nanorods,⁸⁻¹⁰ nanocages,¹¹ and others.¹¹⁻¹⁴ By exposing nanoparticles to la-

Abstract. We describe an application of plasmonic silica/gold nanoshells to produce a controllable laser hyperthermia in tissues with the aim of the enhancement of cancer photothermal therapy. Laser irradiation parameters are optimized on the basis of preliminary experimental studies using a test-tube phantom and laboratory rats. Temperature distributions on the animal skin surface at hypodermic and intramuscular injection of gold nanoparticle suspensions and affectations by the laser radiation are measured *in vivo* with a thermal imaging system. The results of temperature measurements are compared with tissue histology. © 2009 Society of Photo-Optical Instrumentation Engineers. [DOI: 10.1117/1.3122371]

Keywords: nanoparticles; silica/gold nanoshells; plasmon resonance; laser photothermal cancer therapy.

Paper 08288SSRR received Sep. 4, 2008; revised manuscript received Mar. 4, 2009; accepted for publication Mar. 4, 2009; published online Apr. 27, 2009.

ser radiation near their plasmon-resonant absorption band, it is possible to produce local heating of nanoparticle labeled cells without harming surrounding healthy tissues. Such an approach has been developed over the last five years and it has been called plasmonic photothermal therapy (PPTT).¹⁵ The spectral tuning of nanoparticle resonance to the “therapeutic optical window” (750 to 1100 nm) and achieving the desired ratio between the absorption and scattering efficiencies can be achieved by variation in the particle size, shape, and structure.¹⁶⁻²⁰ In practice, almost all reports on PPTT used diode lasers with the wavelength around 805 to 810 nm.

Address all correspondence to: Irina Maksimova, Department of Optics and Biophotonics, Saratov State University, 83 Astrakhanskaya, Saratov 410012 Russia. Tel: +7845-251-3667; Fax: +7845-251-2798; E-mail: irina_mksmv@yahoo.com

Prior to laser treatment, the index matching agents (e.g., PEG diacrylate) may be applied over the tumor surface.²¹

Gold nanoshells (GNSs) belong to a prospective class of optical adjustable nanoparticles with dielectric (silica) core included in a thin metallic (gold) shell.²² By an appropriate choice of the ratio of core diameter to shell thickness and surface functionalization, the so-called immunotargeted GNSs can be engineered that effectively absorb or scatter light at a desired wavelength from visible to infrared, and provide selective labeling of cancer cells.²³ The surface PEGylation of GNSs ensures their stability against agglomeration at physiological conditions during systemic circulation.^{24,25} The absorption cross section of a single GNS is high enough to provide a competition of nanoparticle technology with applications of indocyanine green dye—a typical photothermal sensitizer used in laser cancer therapy.²⁶ Enhanced efficiency of absorption and scattering of GNSs have been used to develop a combined approach, allowing one to provide selective destruction of GNS-labeled carcinoma cells via PPTT and concurrent optical coherence tomography (OCT) imaging of tumor tissues.²⁷

There are several papers on *in vitro* experiments concerning application of NSs to PPTT of cancer cells,^{5,6,28–31} while the number of *in vivo* and *ex vivo* studies is quite limited. Moreover, although several preclinical reports on the utility of GNSs for PPTT and OCT applications are available,^{5,21,32,33} there remain several areas still to be studied more thoroughly. First of all, the question is about controlled and localized hyperthermia without significant overheating of both tumor and surrounding normal tissues. The distribution of elevated temperature under PPTT treatment is determined by absorption of light by nanoparticles acting as point-wise local heat sources, and by thermal diffusion over surrounding tissues. Practically at PPTT one needs to provide the temperature increment ΔT in the range 10 to 20 °C. To achieve these temperature increments, the GNS concentration of (1 to 5) $\times 10^9$ particles/mL, the laser power density of (1 to 5) W/cm², and the treatment exposures between 1 and 5 min were adjusted properly in the published papers. It should be noted that biological effects have nonlinear dependence on changes in the particle concentration and the delivered laser power density, which is defined by the type of tissue and thermoregulation ability of a living organism. A possible method for intelligent PPTT may be adaptive heating in real-time control mode, as described in Ref. 33. Such a technology implies a precise control of local temperature within tumor and surrounding tissues. The use of thermocouples²¹ provides a direct but invasive method, which can be used for laboratory experiments only. In addition, the thermocouples response may be affected by unwanted direct laser heating rather than by the thermal equilibrium with a local tissue volume. More sophisticated and nondirect techniques such as temperature-dependent phase transition of hydrogels³⁴ or ultrasound imaging³⁵ have been recently described. The temperature distribution was also measured by *in vivo* magnetic resonance temperature imaging (MRTI) with the proton-resonance frequency-shift method.^{21,33} The temperature resolution of MRTI measurements is less than 1 °C,

which is close to the resolution of IR thermography. IR thermography is simple and less expensive but is restricted to retrieving surface-temperature data only. It needs the design of special algorithms for reconstruction of in-depth temperature profiles of tissue on the basis of temperature surface measurements.⁴

Precise control over the local temperature distribution is the key factor to be considered in the context of enhanced PPTT efficacy. Laser heating can result in both tumor necrosis (and possibly apoptosis) and in accelerated tumor growth, depending on the accuracy of heating and on the rise in tumor temperature on illumination with laser light. Specifically, heating up to 39 to 45 °C may lead to the acceleration of biological reactions accompanied by the production of shock-heating proteins and by intense growth of the tumor.³⁶ It is generally accepted that one needs to ensure a steep rise in tumor temperature followed by stability over a given time period. The use of plasmon-resonant particles in general meets the basic goals of PPTT related to controllable tumor heating. It is significant that gold nanoparticle light-mediated therapy is on the way to clinical trials in humans; however, extensive animal studies should be done prior.

To characterize tissue heating effects, the morphological investigations in the framework of therapeutic pathomorphology should be provided. Although such an approach has been used for estimation of hyperthermic effects of gold nanorods in tumor cells,⁹ studies of morphological changes under *in vivo* conditions are quite rare^{5,21} and they still need additional efforts to be completely understood.

The present work is focused on the investigation of heating kinetics, spatial temperature distribution, and morphological alterations in tissues dependent on laser irradiation parameters and nanoparticle concentration. We describe experimental results for phantoms and laboratory animals at several temperature regimes and related morphological tissue patterns.

2 Materials and Methods

2.1 Reagents

The following reagents were used to provide protocol of gold nanoparticle synthesis: tetraethyl orthosilicate (TEOS, Aldrich, Saint Louis, Missouri) tetrakis (hydroxymethyl) phosphonium chloride (THPC, Fluka, Saint Louis, Missouri), 3-aminopropyltrimethoxysilane (APTMS, Aldrich), PEG-thiol (Nektar, San Carlos, California), absolute ethanol, tetrachloroauric acid (TCAA, Aldrich), potash (Reachim Company, Russia), and formaldehyde (Serva, Heidelberg, Germany). All chemicals were of research grade, and 25% aqua ammonia was of analytical grade. Ethanol was purified by additional distillation.

2.2 Gold Nanoparticle Characteristics and Quality Control

For experiments described in this work, the plasmonic nanoparticles (gold nanospheres and nanoshells) were fabricated in the Laboratory of Nanobiotechnology at the Institute of Biochemistry and Physiology of Plants and Microorganisms (IBPPM) RAS. The poly (ethylene glycol) molecules have been attached (using end thiol groups) to the surface of nano-

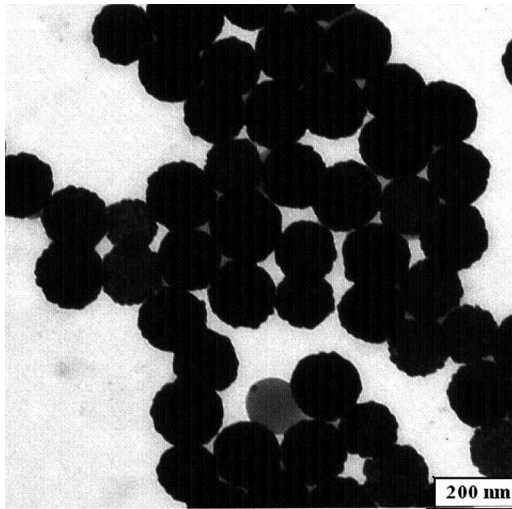


Fig. 1 TEM microgram of suspensions of silica/gold nanoshells, 140/20 nm.

particles to provide their defense from reticuloendothelial systems of the organisms under study.

Silica/gold nanoshells were fabricated as described in paper Ref. 37, with minor modifications related to reagent concentrations. First, silica nanoparticles were grown by reducing TEOS with NH_4OH in absolute ethanol. To do this, we mixed 10 ml of absolute ethanol with 0.6-ml 25% aqua ammonia and 0.3-ml TEOS. For the preparation of gold seeds, 220 μl of 1-M aqueous NaOH and 6 μl of 80% THPC were added to 20 ml of triply distilled water. The solution was vigorously agitated on a magnetic stirrer at 1000 rpm, and after that 880 μl of a 1% TCAA solution were added. Next, aminated silica particles were added to the gold-seed dispersion. Gold particles adsorb to the amine groups on the silica surface, resulting in silica nanoparticle covering by the gold colloid. Gold nanoshells were then grown by reacting HAuCl_4 with

the silica/gold colloid particles in the presence of formaldehyde at room temperature. In this process, additional gold reduces on the adsorbed metal particles, which act as nucleation sites. The nanoshells were centrifuged and sonicated in HPLC-grade water before use.

The following PEGylation protocol was used for silica/gold nanoshells. The nanoshells' solution was centrifuged at 7000 g for 20 min to pellet the particles, decanted, and then nanoshells were resuspended in the same amount of water. One hundred microliters of 2-mM potassium carbonate and 10 μl of 1-mM PEG-thiol solution were added per 1 ml of the nanoparticles' solution. The mixture was stored overnight at room temperature, then the centrifuged, decanted, and prepared PEGylated nanoshells were resuspended in water several times to remove the PEG-thiol excess.

Nanoshells have silica cores of 140 nm in diameter with 20-nm-thick gold shells. These parameters have been chosen to provide plasmon resonance in the IR region of the spectrum where diode lasers radiate.

Parameters of fabricated gold nanoparticles were tested by spectral analysis (measuring of optical density) and by transmission electron microscopy (TEM). The average diameter of nanoshells of 160 nm was evaluated using TEM micrograms of nanoshell suspensions (Fig. 1). Synthesized nanoshell suspensions had a sufficient narrow size distribution.

Spectral characteristics of gold nanoparticles calculated using the Mie theory are presented in Fig. 2(a). Solid gold nanospheres of 15 and 50 nm in diameter have extinction maximums at the wavelengths near 520 nm. Optical properties of such particles are characterized by strong absorption and weak scattering. For providing tissue hyperthermia by 810-nm laser diode, the best is using gold nanoshells with the ratio of core diameter to shell thickness as 140/20 nm, because these particles have extinction maximums at this particular wavelength, which fits well with the optical transparency window of the tissue. The measured spectrum of optical

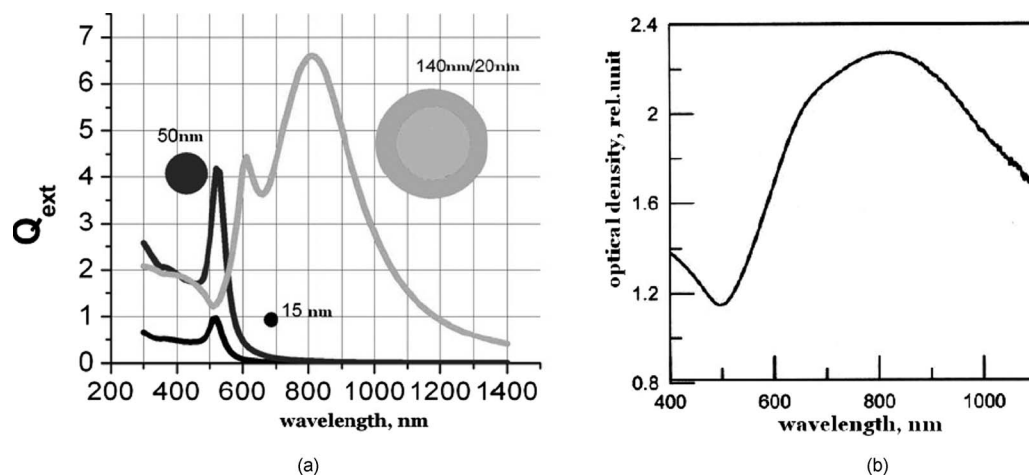


Fig. 2 (a) Theoretical spectral curves of extinction cross section for gold nanoparticles of 15 and 50 nm in diameter, and silica/gold nanoshells (140/20 nm). (b) Experimental spectral curve of optical density for silica/gold nanoshells (140/20 nm).

density of fabricated silica/gold nanoshells is presented in Fig. 2(b). There is a good correlation between calculated and measured spectra; however, the experimental curve is smoother due to particle size heterogeneity.

2.3 Animals

For *in vivo* experiments, the white laboratory rats, 8 to 10 weeks of age (weight 180 to 200 g), were used. Animals were bred under SPF conditions and a barrier was maintained for animals involved in experiments. Drinking water and conventional food were provided *ad libitum*. Husbandry conditions were maintained according to all applicable provisions of the national laws. The experimental protocol was approved by an independent ethical committee prior to the study.

2.4 Experimental Design

Investigation of thermal effects and alterations of tissue morphology induced by laser irradiation at subcutaneous and/or intramuscular injection of 0.1-ml silica/gold nanoshell suspensions was carried out using white laboratory rats. In solution of designed silica/gold nanoshells (140/20 nm), gold content was of 150 $\mu\text{g}/\text{ml}$. Similar concentration expressed in the number of particles, $N=5 \times 10^9 \text{ cm}^{-3}$, was used in *in vitro* experiments with tissue phantoms. In *in vivo* studies, 48 animals were divided into two groups, 24 rats in each; rats from the first and the second groups were irradiated by continuous wave (cw) and pulse laser light, accordingly. Each of the 24 animals in each group was injected with a solution of gold nanoparticle suspension once subcutaneously and then in 20 min intramuscularly. The first injection was done subcutaneously in front of the abdominal wall, the second intramuscular one was done into the hip far enough from the first injection area. After two minutes elapsed after each injection, the skin area around the injection puncture was exposure to laser light to produce photothermal effects mediated by the inserted nanoparticles within the skin or within the muscle tissue. A 20-min delay and different locations of treated areas allowed us to consider tissue photothermal responses at subcutaneous and intramuscular gold nanoparticle delivery for the particular animal as independent ones. We used the diode laser from Opto Power Corporation (Tusca, Aricon), providing a mean wavelength of 810 nm, optical-fiber output, and cw and pulse regimes. The cw laser output power was 2 W. In pulse mode, peak power was 8 W, with an on-off time ratio of 0.25, and pulse duration of 1 msec. The preliminary estimation of heating kinetics and size of the heated area was carried out at different concentrations of nanoparticles in a test tube. For noninvasive measurement of spatial distribution of surface temperature of objects under investigation, the IR Imager IRISYS 4010, Infrared Integrated System Limited (Northampton, United Kingdom) was used. General anesthesia was used for providing experiments *in vivo*. Tissue samples for histological examination were collected after injection of nanoparticles before, after, and 24-hr past laser heating. Heating duration was from 10 to 360 sec. To prove

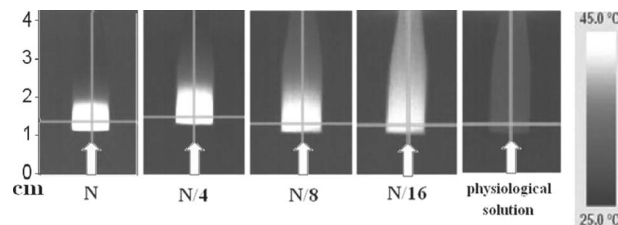


Fig. 3 Thermograms of the test tube containing solutions of silica/gold nanoshells (140/20 nm) and physiological solution of heating by diode laser (810 nm). Maximal particle concentration is $N=5 \times 10^9 \text{ cm}^{-3}$.

the evidence of nanoparticle delivery into the tissue and to evaluate qualitatively their spatial distribution within the tissue, TEM and dark-field optical microscopy were used.

2.5 Imaging of Gold Nanoparticles

The dark-field optical microscopy was used for imaging of gold nanoparticles in tissue slices [Biolam-M microscope (LOMO, Saint Petersburg, Russia)].

For electron microscopic examinations, the cut-out strips of tissue of size $3 \times 5 \text{ mm}$ were rapidly ground by blade to pieces not more than $1 \times 1 \text{ mm}$. Further fixation, dehydration, and subsequent impregnation with resin via standard procedures were carried out. Tissue thin slices were obtained by the ultratome Reichert (Austria), and thickness was from 40 to 80 nm. Each slice was mounted to the grids without the base layers and contrasted by the saturated alcoholic solution of uranyl acetate at a temperature of 56 $^{\circ}\text{C}$ during 10 min. Specimens were investigated using a Hitachi Hu-1a electron microscope (Japan) in transmission microscopy (TEM) mode.

Diffuse backscattering spectroscopy at the application of fiber optic spectrometer LESA-01 was used for noninvasive *in vivo* detecting of subcutaneously injected gold nanoparticles. The sample was illuminated with the source fiber (fiber core diameter of 200 μm), and diffuse reflected light was collected with six detector optical fibers (200 μm), which were $\sim 0.3 \text{ mm}$ apart from the source fiber. Distance between the fiber probe tip and skin was 0.5 mm. The detector fibers were coupled to a spectrometer, and a diffuse reflectance spectrum was collected over a wavelength range of 450 to 1000 nm. Prior to spectral analysis, recorded signals were corrected for system response.

2.6 Thermography

An IR thermograph was used for noninvasive monitoring of surface temperatures. The thermal imaging system IRISYS 4010 is based on the uncooled bolometric matrix providing temperature recording in the range from -10 to $+250 \text{ }^{\circ}\text{C}$, with sensitivity of $0.15 \text{ }^{\circ}\text{C}$. The system is sufficiently fast (8 frames per second) to provide animal studies *in vivo*. The memory flash of the thermal imager makes it possible to record up to 6000 thermograms with 120×160 pixel size. Range of focus is from 30 cm to infinity. The minimal size of the object, whose temperature can be measured, depends on

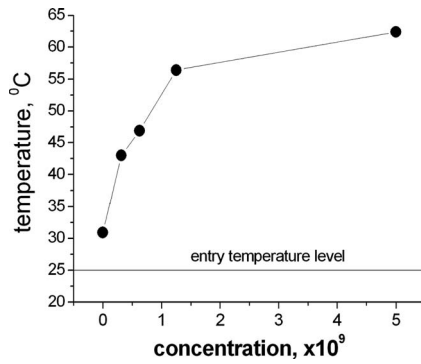


Fig. 4 Maximal temperature of gold nanoparticle solution with different concentrations measured at the end of cw laser irradiation within 2 min (power 2 W, total energy 120 J, power density 4 W/cm²).

the distance between the IR imager and the object. The wavelength range of the thermal imager comprises 8 to 14 μm , thus the scattered laser radiation (810 nm) does not affect thermal-vision measurements.

3 Results

3.1 Model Experiments on Near Infrared Laser Heating Mediated by Gold Nanoparticles

A preliminary investigation using phantom studies and computer simulations are necessary to solve the inverse problem of reconstruction of in-depth temperature distribution on the basis of surface thermal imaging for the specified experimental conditions. For optimization of laser heating technology, in-depth temperature distributions were investigated using 2-ml test tubes (1 cm diam) containing solutions of silica/gold nanoshells (140/20 nm) with different concentrations (Fig. 3). Heating was provided at irradiating by a cw NIR diode laser (810 nm) for 2 min (total dose of 120 J, power density 4 W/cm²). From the measurements, it follows that at high concentrations of particles the whole phantom volume is not heated directly by laser light, but only the part which is closer to the incident laser beam. The rest volume of nanoparticle solution is heated up indirectly due to a thermal diffusion process. Thus, inhomogeneity of heating could be expected. With lesser concentration of particles, the whole volume is heated directly by laser light, but this heating could be insufficient. Evident inhomogeneity of in-depth heating of nanoparticle solutions is followed from data presented in Fig. 3. The effective heating depth for highly concentrated solutions ($N=5 \times 10^9 \text{ cm}^{-3}$) does not exceed 5 to 7 mm. This puts restrictions on nanoparticle concentration for clinical applications for tumors with sizes bigger than 1 cm³. If the concentration decreases four times, the effective heating depth is increased two times. Uniform temperature distribution in the test tube is recorded only at the thinning of the nanoparticle solution 16 times. In this case, maximal temperature alterations do not exceed 18 $^{\circ}\text{C}$, while at a concentration of $5 \times 10^9 \text{ cm}^{-3}$, temperature rise is 40 $^{\circ}\text{C}$. It is necessary to

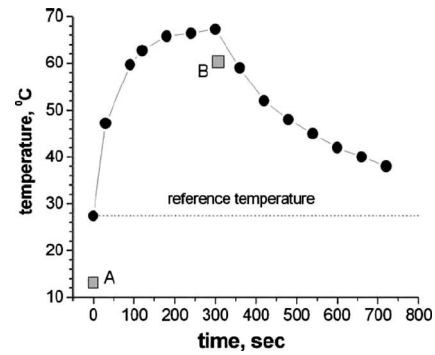


Fig. 5 Temporal dependence of temperature in the center of the laser spot of the cw (4 W/cm²) diode laser (810 nm) used for heating the solution of gold nanoparticles with a concentration of $N=5 \times 10^9 \text{ cm}^{-3}$ in the test tube.

note that 810-nm laser radiation is also absorbed by water, thus in control measurements with the test tube filled up by physiological solution, background heating was about 6 $^{\circ}\text{C}$.

The temperature measurements using a test tube allowed us to determine the upper limit of the temperature increase in tissues. The concentration of gold nanoparticles in tissues is conceivably lower than in the initial injected solution. To estimate temperature rise in tissues, experimental dependence of temperature rise on concentration of gold nanoparticles in a phantom can be used (see Fig. 4). Temperature kinetics for the solution of gold nanoparticles with a concentration of $N=5 \times 10^9 \text{ cm}^{-3}$ is shown in Fig. 5. The observed temporal dependence of temperature rise is nonlinear. The most heating occurs over the first 100 sec of laser irradiation, then temperature increase is saturated with time. After laser switch off, the temperature decreases more slowly than it increased at laser heating. Even after 5 min elapsed since the laser was switched off, the temperature of nanoparticle solution was about 10 $^{\circ}\text{C}$ above the reference one. Evidently, the cooling rate depends on the thermal diffusivity of material and sample volume. The characteristic thermal time response of an object is defined by its dimension R_o (the radius for a cylinder form) and the thermal diffusivity of its material a_T :⁴

$$\tau_T \sim (R_o)^2/a_T. \quad (1)$$

Experimental values for the thermal diffusivity a_t of many soft tissues lie within the rather narrow range from $1.03 \times 10^{-7} \text{ m}^2/\text{s}$ (hydrated collagen containing 50% of water) to $1.46 \times 10^{-7} \text{ m}^2/\text{s}$ (pure water). Therefore, the characteristic thermal time response for our experiments with phantoms and tissues according to expression (1) is around 200 to 300 sec. This value is in good agreement with our experimental results presented in Fig. 5. Therefore, the real time of object overheating exceeds the laser exposure time. This finding is necessary to take into account to assign a duration of local laser hyperthermia mediated by gold nanoparticles.

3.2 In Vivo Near-Infrared Laser Hyperthermia Mediated by Gold Nanoshells

These experimental studies aim the *in vivo* determination of the spatial distributions of temperature corresponding to dif-

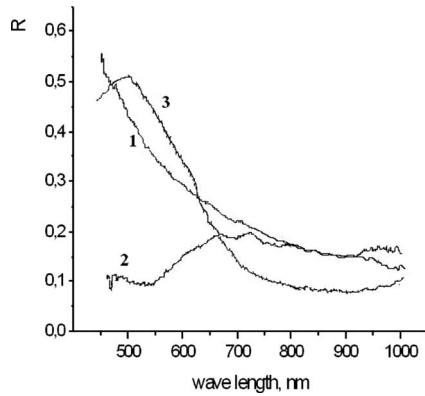


Fig. 6 Diffuse reflectance spectra of rat skin: 1—skin without nanoparticles; 2—subcutaneously injected gold nanoparticles of 15 nm in diameter; and 3—subcutaneously injected silica/gold nanoshells (140/20 nm).

ferent depths and concentrations of nanoparticles in tissues of white laboratory rats. The solution of silica/gold nanoshells (140/20 nm, 150 $\mu\text{g}/\text{ml}$ of gold) was injected (0.1 ml) subcutaneously or intramuscularly. The diffuse backscattering spectrum of the skin as a scattering medium is influenced by inserted gold nanoparticles due to the specific absorption spectrum of the particles (see Fig. 2). Evidently, the effect of nanoparticles on the backscattering spectrum should be lower as the depth of the layer of the inserted gold nanoparticles increases. Experimental diffuse reflectance spectra measured for rat skin with injected gold nanoparticles (Fig. 6) validate the possibility to detect gold nanoparticles within some depth in tissue. These spectra are different from the absorption spectrum of gold nanoparticle solution. The maximum of diffuse reflectance of the skin with gold nanoparticles is mismatched with the absorbance peak of gold colloid. The rise of backscattering intensity (curve 3) nearly 530 nm for tissue with nanoshells is due to the backscattering of these particles. The absorption peaks [$\lambda=530$ nm for particles with 15-nm size

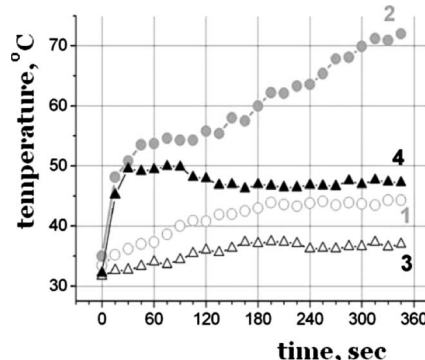


Fig. 7 *In vivo* measured temporal dependences of rat skin temperature at cw (●,○) and pulse (△,△) laser heating, 1, 3—without nanoparticles, 2, 4—with silica/gold nanoshells (140/20 nm), subcutaneous injection.

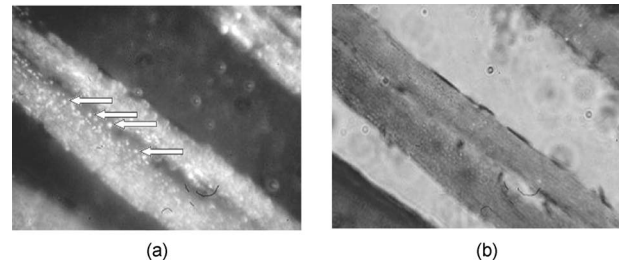


Fig. 8 Histological study of muscle tissue (200 \times). Staining by hematoxylin/eosin: (a) dark-field image and (b) optical transmission image. The white arrows show the gold particle clusters.

and $\lambda=810$ nm for nanoshells with 140/20-nm size (Fig. 2)] correspond to the minimal values (dips) of diffuse backscattering spectra. This dips are formed because of nanoparticle absorption of scattered radiation in inhomogeneous medium.

In vivo temperature spatial distributions were measured for cw and pulsed laser irradiation and different injection depths of nanoparticles into tissues (Fig. 7). It is seen that heating is happening more rapidly and temperature rise is substantially higher at laser irradiation of the skin with inserted nanoparticles than for skin free of particles. The rate of heating is very important for photothermal therapy of cancer. Temperature rise to 46 to 50 $^{\circ}\text{C}$ is accepted as optimal for this purpose.³⁸ Such temperatures admittedly stimulate apoptosis in tumor tissue, in contrast to heating in the range 37 to 43 $^{\circ}\text{C}$, which is very undesirable.³⁹ In our experiments, by using nanoshells the time interval for tissue heating up to 46 $^{\circ}\text{C}$ was 15 to 20 sec, and in their absence it was more than tenfold prolonged, up to 3 to 4 min.

It is interesting to note that both temperature kinetic curves for cw and pulsed irradiation of tissue with nanoparticles have a local maximum at 60 sec (Fig. 7). The origin of this maximum may be explained by the manifestation of compensatory reaction of organisms to temperature rise, which has a characteristic time of about 100 sec. With the fast heating caused by nanoparticles, the inertial mechanism of heat regulation could not provide any immediate temperature compensation. In contrast, essentially good compensation is realized for laser heating without inserted particles, and some compensation is seen in a larger time scale for heating with inserted nanoparticles. Also important to note is that laser pulse heating is more controllable in a large time scale and has similar short time kinetics as cw. In that sense, pulsed irradiation could be preferable because it gives fast and self-limited temperature rise. The comparison of curves 2 and 4 (Fig. 7) shows that the increase of effectiveness of hyperthermia is possible by a combination of different heating modes. It is reasonable to use the prime cw mode with a higher power density of laser radiation, and switch over to pulse mode or cw mode with lower power.

At 24 h after laser action, biopsy samples of irradiated tissues were taken for histological investigation. Dark-field microscopy was used for imaging of nanoparticles in muscle tissue (Fig. 8).

In vivo thermal measurements and histological studies of the tissue before and after laser irradiation were compared.

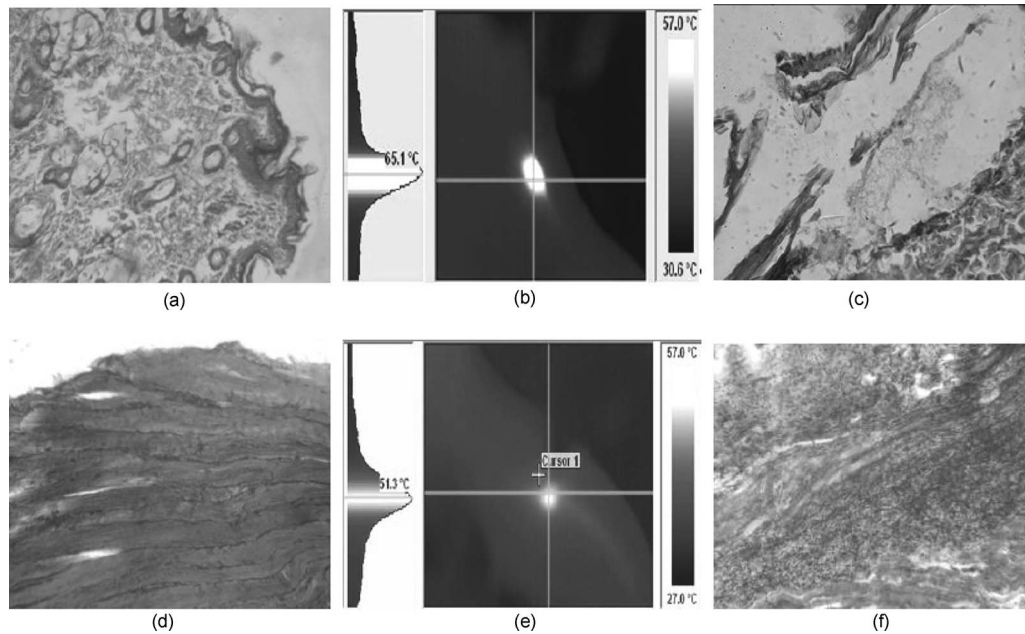


Fig. 9 Comparison of local temperature rise and corresponding alterations in tissue morphology: (a) histology of rat skin before laser action, (b) thermogram at laser heating with subcutaneous administration of silica/gold nanoshells (140/20 nm), (c) histology of rat skin after 30 sec of laser action, (d) histology of rat muscle tissue before laser action, (e) thermogram at laser heating with intramuscular administration of silica/gold nanoshells (140/20 nm), and (f) histology of rat muscle tissue after 30 sec of laser action.

Figure 9 shows the thermograms and structure of the skin and muscle tissue before and after laser action on tissue with the administrated nanoshells.

In the control samples, we did not observe any pathological changes [Figs. 9(a) and 9(d)]. For subcutaneously administrated nanoshells after laser irradiation, epidermis of the skin is partly absent with the formation of vesicles filled up by serous fluid. In the derma, we found severe edema with disorientation of collagen fibers [Fig. 9(c)]. In the muscle tissue we observed edema, hyperemia, and inflammatory infiltration by leukocytes. The control of the spatial distribution of the temperature of the skin surface using the IR imager showed that after 30 sec of laser action, the maximal temperature in the center of the laser spot is about 65 °C [Fig. 9(b)].

At intramuscular administration of the nanoshells, we revealed moderate edema with defibrillation of collagen fibers

in muscle tissue [Fig. 9(f)]. In the connective tissue, we observed inflammatory leukocyte infiltration and edema. In the case of intramuscular particle introduction, we did not observe significant changes in color or structure of tissue surface during the irradiation time. However, the surface temperature was approximately 7 °C higher than in the control measurements without nanoparticles. Thus, the laser thermolysis can be achieved in the region of nanoparticle localization without damage of the surface tissues. This conclusion is confirmed by histological examinations.

Figure 10 shows aggregates (clusters) of nanoshells (marked by white arrows) injected immediately in tissue before laser action. There are evident signs of cell damage: the nucleus contains vacuoles (V), the cytoplasmic membrane (CM) is ruinous, and cytoplasm is pouring out into extracellular space. Near the cell there are unstructured necrotic masses (NM), maybe remains of destroyed cells.

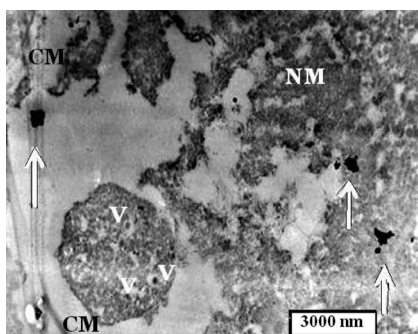


Fig. 10 TEM image of skin after subcutaneous injection of nanoparticles and laser irradiation.

4 Conclusion

Gold nanoshells with maximum extinction in the NIR spectral range are synthesized. Spectral characteristics of design nanoparticles are in good agreement with theoretical ones calculated on the basis of the Mie theory. Parameter verification (size and shape) is executed by TEM. By experimental investigations using a test tube, the dependences of temperature rise of solutions on concentration of nanoparticles are measured, as well as the depth and time interval of laser heating. It is found that at cw laser heating, the time needed to reach the steady-state temperature conditions is 100 to 150 sec. The results of studying laser heating kinetics allow us to optimize clinical protocol for cancer treatments via inducing pathologi-

cell apoptosis or their photothermolysis by NIR laser irradiation. For instance, both cw and pulse laser heating have similar short time kinetics (temperature rise up to 46 to 50 °C over time no more than 40 sec); however, due to compensatory response of the organism, pulsed laser heating is more controllable than cw on a large time scale. In that sense, pulsed irradiation (on-off time ratio of 0.25, and pulse duration of 1 msec) is preferable because it gives fast and prolonged self-limited temperature rise. Temperature distributions and corresponding morphological alterations in tissues caused by laser heating at different depths of inserted nanoparticles are analyzed. Gold nanoshells mediated laser destruction of muscle tissue is achieved *in vivo* in the region of nanoparticle localization (at a depth of 4 mm) without any damage to surface tissues. In spite of similar power densities used in pulse and cw mode, the nanoparticle mediated laser heating of tissue is different in these two modes. The combined mode of laser operation for optimization of laser heating could be useful. It is found that the elevated temperature of the object under study is kept for some time after laser action. This finding is necessary to account for assigning duration of local laser/gold nanoparticle hyperthermia in clinical studies. The presented results allow us to estimate the concentration of nanoparticles needed for providing desirable temperature elevation and the potentiality of controllable laser hyperthermia of deep tissue layers without damage to overlying tissue layers. In particular, optimal nanoparticle concentration that provides smooth heating of tissue volume allows for the treatment of tumors with sizes no bigger than 1 cm³. Thus, to provide smooth heating of big tumors at high concentrations of nanoparticles, multibeam irradiation could be effective.

The back reflectance spectral measurements demonstrate the possibility of *in vivo* visualization of nanoparticle-filled tissue regions within the depth of at least a few millimeters from the skin surface. Therefore, fiber optic diffuse spectroscopy is a promising tool for noninvasive monitoring of selective accumulation of nanoparticles in tumors in clinical studies.

Acknowledgments

This research was supported by grants of RFBR (numbers 07-02-01434a and 08-02-00399a), RF Program on the Development of High School Potential (number 2.1.1/4989 and 2.2.1.1/2950), the President of the RF for the support of Leading Scientific Schools (number 208.2008.2), FP7-ICT-2007-2 PHOTONICS4LIFE (number 224014). B. Khlebtsov was supported by grants from the President of the Russian Federation (MK) and RFBR (numbers 07-04-00301a, 07-04-00302a, and 09-02-00496-a). N. Khlebtsov was supported by a grant from the Presidium of RAS Program "The Basic Sciences—to Medicine."

References

1. G. Müller and A. Roggan, *Laser-Induced Interstitial Thermotherapy*, **PM25**, SPIE Press, Bellingham, WA (1995).
2. P. Wust, B. Hildebrandt, G. Sreenivasa, B. Rau, J. Gellermann, H. Riess, R. Felix, and P. M. Schlag, "Hyperthermia in combined treatment of cancer," *Lancet Oncol.* **3**, 487–497 (2002).
3. H. P. Berlien and G. J. Mueller, *Applied Laser Medicine*, Springer-Verlag, Berlin (2003).
4. V. V. Tuchin, *Tissue Optics: Light Scattering Methods and Instru-*

ments for Medical Diagnosis, 2nd ed., **PM 166**, SPIE Press, Bellingham, WA (2007).

5. L. R. Hirsch, R. J. Stafford, J. A. Bankson, S. R. Sershen, B. Rivera, R. E. Price, J. D. Hazle, N. J. Halas, and J. L. West, "Nanoshell-mediated near-infrared thermal therapy of tumors under magnetic resonance guidance." *Proc. Natl. Acad. Sci. U.S.A.* **100**, 13549–13554 (2003).
6. C. Loo, A. Lin, L. Hirsch, M. Lee, J. Barton, N. Halas, J. West, and R. Drezek, "Nanoshell-enabled photonics-based imaging and therapy of cancer," *Technol. Cancer Res. Treat.* **3**, 33–40 (2004).
7. I. L. Maksimova, G. G. Akchurin, B. N. Khlebtsov, G. S. Terentyuk, G. G. Akchurin (Jr.), I. A. Ermolaev, A. A. Skaptsov, E. P. Soboleva, N. G. Khlebtsov, and V. V. Tuchin, "Near-infrared laser photothermal therapy of cancer by using gold nanoparticles: computer simulations and experiment," *Med. Laser Appl.* **22**, 199–206 (2007).
8. X. Huang, I. H. El-Sayed, W. Qian, and M. A. El-Sayed, "Cancer cell imaging and photothermal therapy in the near-infrared region by using gold nanorods," *J. Am. Chem. Soc.* **128**, 2115–2120 (2006).
9. T. B. Huff, L. Tong, Y. Zhao, M. N. Hansen, J. X. Cheng, and A. Wei, "Hyperthermic effects of gold nanorods on tumor cells," *Nanomedicine* **2**, 125–132 (2007).
10. E. B. Dickerson, E. C. Dreaden, X. Huang, I. H. El-Sayed, H. Chu, S. Pushpanketh, J. F. McDonald, and M. A. El-Sayed, "Gold nanorod assisted near-infrared plasmonic photothermal therapy (PPTT) of squamous cell carcinoma in mice," *Cancer Lett.* **269**, 57–66 (2008).
11. J. Chen, D. Wang, J. Xi, L. Au, A. Siekkinen, A. Warsen, Z. Y. Li, H. Zhang, Y. Xia, and X. Li, "Immuno gold nanocages with tailored optical properties for targeted photothermal destruction of cancer cells," *Nano Lett.* **7**, 1318–1322 (2007).
12. P. K. Jain, I. H. El-Sayed, and M. A. El-Sayed, "Au nanoparticles target cancer," *Nanotoday* **2**, 18–29 (2007).
13. D. Pissuwan, S. M. Valenzuela, and M. B. Cortie, "Therapeutic possibilities of plasmonically heated gold nanoparticles," *Trends Biotechnol.* **24**, 62–67 (2006).
14. R. Visaria, J. C. Bischof, M. Loren, B. Williams, E. Ebbini, G. Paciotti, and R. Griffin, "Nanotherapeutics for enhancing thermal therapy of cancer," *Int. J. Hyperthermia* **23**, 501–511 (2007).
15. X. Huang, P. K. Jain, I. H. El-Sayed, and M. A. El-Sayed, "Plasmonic photothermal therapy (PPTT) using gold nanoparticles," *Lasers Med. Sci.* **23**, 217–228 (2008).
16. S. Oldenburg, R. D. Averitt, S. Westcott, and N. J. Halas, "Nanoengineering of optical resonances," *Chem. Phys. Lett.* **288**, 243–247 (1998).
17. B. N. Khlebtsov, V. P. Zharov, A. G. Melnikov, V. V. Tuchin, and N. G. Khlebtsov, "Optical amplification of photothermal therapy with gold nanoparticles and nanoclusters," *Nanotechnology* **17**, 5167–5179 (2006).
18. N. Harris, M. J. Ford, and M. B. Cortie, "Optimization of plasmonic heating by gold nanospheres and nanoshells," *J. Phys. Chem. B* **110**, 10701–10707 (2006).
19. N. G. Khlebtsov, "Optics and biophotonics of nanoparticles with a plasmon resonance," *Quantum Electron.* **38**, 504–529 (2008).
20. V. Myroshnychenko, J. Rodriguez-Fernandez, I. Pastoriza-Santos, A. M. Funston, C. Novo, P. Mulvaney, L. M. Liz-Marzan, and F. J. Garcia de Abajo, "Modelling the optical response of gold nanoparticles," *Chem. Soc. Rev.* **37**, 1792–1805 (2008).
21. P. Diagaradjane, A. Shetty, J. C. Wang, A. M. Elliott, J. Schwartz, S. Shentu, H. C. Park, A. Deorukhkar, R. J. Stafford, S. H. Cho, J. W. Tunnell, J. D. Hazle, and S. Krishnan, "Modulation of *in vivo* tumor radiation response via gold nanoshell-mediated vascular-focused hyperthermia: characterizing an integrated antihypoxic and localized vascular disrupting targeting strategy," *Nano Lett.* **8**, 1492–1500 (2008).
22. L. R. Hirsch, A. M. Gobin, A. R. Lowery, F. Tam, R. A. Drezek, N. J. Halas, and J. L. West, "Metal nanoshells," *Ann. Biomed. Eng.* **34**, 15–22 (2006).
23. P. K. Jain, K. S. Lee, I. H. El-Sayed, and M. A. El-Sayed, "Calculated absorption and scattering properties of gold nanoparticles of different size, shape, and composition: applications in biological imaging and biomedicine," *J. Phys. Chem. B* **110**, 7238–7248 (2006).
24. R. T. Zaman, P. Diagaradjane, J. C. Wang, J. Schwartz, N. Rajaram, K. L. Gill-Sharp, S. H. Cho, H. G. Rylander III, J. D. Payne, S. Krishnan, and J. W. Tunnell, "In vivo detection of gold nanoshells in tumors using diffuse optical spectroscopy," *IEEE J. Sel. Top. Quantum Electron.* **13**, 1715–1720 (2007).

25. B. Kogan, N. Andronova, N. Khlebtsov, B. Khlebtsov, V. Rudoy, O. Dement'e'eva, E. Sedykh, and L. Bannykh, "Pharmacokinetic study of PEGylated plasmon resonant gold nanoparticles in tumor-bearing mice," *Tech. Proc. 2008 NSTI Nanotechnol. Conf. Trade Show, NSTI-Nanotech, Nanotechnol.* **2**, 65–68 (2008).
26. V. G. Liu, T. M. Cowan, S. W. Jeong, S. L. Jacques, E. C. Lemley, and W. R. Chen, "Selective photothermal interaction using an 805-nm diode laser and indocyanine green in gel phantom and chicken breast tissue," *Lasers Med. Sci.* **17**, 272–279 (2002).
27. A. M. Gobin, M. H. Lee, N. J. Halas, W. D. James, R. A. Drezek, and J. L. West, "Near-infrared resonant nanoshells for combined optical imaging and photothermal cancer therapy," *Nano Lett.* **7**, 1929–1934 (2007).
28. C. Loo, A. Lowery, N. Halas, J. West, and R. Drezek, "Immunotargeted nanoshells for integrated cancer imaging and therapy," *Nano Lett.* **5**, 709–711 (2005).
29. R. J. Bernardi, A. R. Lowery, P. A. Thompson, S. M. Blaney, and J. L. West, "Immunonanoshells for targeted photothermal ablation in medulloblastoma and glioma: an *in vitro* evaluation using human cell lines," *J. Neuro-Oncol.* **86**, 165–172 (2008).
30. T. S. Hauck and W. C. W. Chan, "Gold nanoshells in cancer imaging and therapy: towards clinical application," *Nanomedicine* **2**, 735–738 (2007).
31. A. R. Lowery, A. M. Gobin, E. S. Day, N. J. Halas, and J. L. West, "Immunonanoshells for targeted photothermal ablation of tumor cells," *Int. J. Nanomed.* **1**(2), 149–154 (2006).
32. D. P. O'Neal, L. R. Hirsch, N. J. Halas, J. D. Payne, and J. L. West, "Photo-thermal tumor ablation in mice using near infrared-absorbing nanoparticles," *Cancer Lett.* **209**, 171–176 (2004).
33. Y. Feng, D. Fuentes, A. Hawkins, J. Bass, M. N. Rylander, A. Elliott, A. Shetty, R. J. Stafford, and J. T. Oden, "Nanoshell-mediated laser surgery simulation for prostate cancer treatment," *Eng. Comput.* **25**(1), 3–13 (2009).
34. M. Bikram, A. M. Gobin, R. E. Whitmire, and J. L. West, "Temperature-sensitive hydrogels with SiO₂-Au nanoshells for controlled drug delivery," *J. Controlled Release* **123** 219–227 (2007).
35. J. Shah, S. R. Aglyamov, K. Sokolov, T. E. Milner, and S. Y. Emelianov, "Ultrasound imaging to monitor photothermal therapy—feasibility study," *Opt. Express* **16**, 3776–3785 (2008).
36. W. L. Yang, D. G. Nair, R. Makizumi, G. Gallos, X. Ye, R. R. Sharma, and T. S. Ravikumar, "Heat shock protein 70 is induced in mouse human colon tumor xenografts after sublethal radiofrequency ablation," *Ann. Surg. Oncol.* **11**, 399–406 (2004).
37. S. L. Westcott, S. J. Oldenburg, T. R. Lee, and N. J. Halas, "Formation and Adsorption of gold nanoparticle-cluster on functionalized silica nanoparticle surfaces," *Langmuir* **14**, 5396–5401 (1998).
38. K. Ivarsson, L. Myllymäki, K. Jansner, U. Stenram, and K. G. Tranberg, "Resistance to tumour challenge after tumour laser therapy is associated with a cellular immune response," *Br. J. Cancer* **93**, 435–440 (2005).
39. S. Basu, R. J. Binder, R. Suto, K. M. Anderson, and P. K. Srivastava, "Necrotic but not apoptotic cell death releases heat shock proteins, which deliver a partial maturation signal to dendritic cells and activate the NF-kappaB pathway," *Int. Immunol.* **12**, 1539–1546 (2000).